

Performance model of imaging FTS as a standoff chemical agent detection tool

Martin Chamberland^{*a}, Vincent Farley^a, Pierre Tremblay^b, Jean-François Legault^a

^aTelops inc., 4940 Pierre-Georges-Roy, St-Augustin, Qc, Canada G3A 1V7

^bElectrical Engineering Dept, Université Laval, Québec, Qc, Canada G1K 7P4

ABSTRACT

Standoff detection of chemical agents may be enhanced with the capability to measure an image of the agent concentration. The use of an imaging Fourier-Transform Spectrometer to perform these measurements is extensively modeled in order to predict its ultimate capabilities. The model developed allows one to determine the optimal configuration of the instrument, taking into account the precise characteristics of realistic and existing hardware.

The model is first based on the calculation of radiative transfer from the scene into the instrument up to the imaging detector. Standard performance models of FTS are improved to include the particular features of imaging FTS operated with infrared cameras. The infrared focal plane arrays have their own constraints that are taken into account in the model.

Keywords: Imaging FTS, chemical agent detection, NESR, NEdT

1. INTRODUCTION

This paper presents the different key items to be considered when modeling the performance of an imaging FTS (Fourier Transform Spectrometer) as a passive standoff chemical agent detection tool. The radiative transfer from the scene up to the imaging detector is the first presented item. Secondly, we present the technical constraints imposed by the use of an FPA (Focal Plane Array) to the design and operating parameters of the instrument. We also present how to model the noise from sampling jitter, predict the modulation efficiency for uncompensated systems and calculate the ILS (Instrument LineShape) for the various pixels. Finally, NEdT is presented for a typical configuration.

1.1. Imaging FTS system overview

The system block diagram of an imaging FTS is presented in Figure 1.

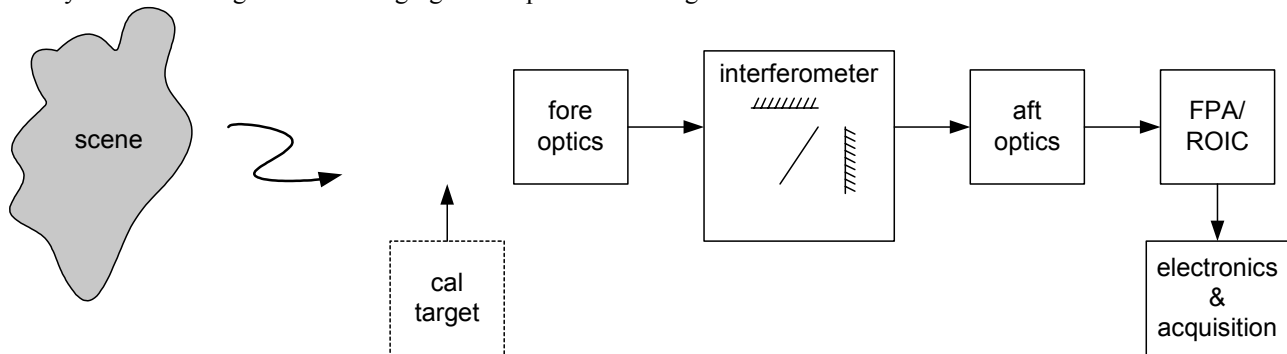


Figure 1: Imaging FTS system block diagram.

The fore optics comprises all the optical components required before the entrance of the interferometer. For some systems, this can be as simple as nothing, while for others, it includes a combination of any of the following items: a pointing mirror, a telescope and collimator, and an entrance window. As far as performance modeling is concerned, the main parameters we need to know on the fore optics are the étendue, the optical transmittance and its temperature.

^{*} martin.chamberland@telops.com; phone (418) 864-7808; www.telops.com

The interferometer contains as a minimum a beamsplitter and 2 mirrors (flat mirror or cube corners). A compensator plate can be used and we present in section 6 some drawbacks of uncompensated systems. In addition to the étendue, the optical transmittance and its temperature, operating parameters like the sweep speed and speed stability, the sampling OPD (optical path difference), the MPD (maximum optical path difference) and the wavefront effects (wavefront tilt, wavefront shear, wavefront error) are essential inputs to predict the performance.

The aft optics contains the lens assembly to focus the beam onto the FPA. An optical relay can be used to locate the entrance pupil such that the size of a critical optical component is minimized for a given étendue. The parameters to determine for modeling are the same as the ones from the fore optics, namely the étendue, the optical transmittance and its temperature.

The FPA has some key optical components. Figure 2 shows a typical layout of a FPA.

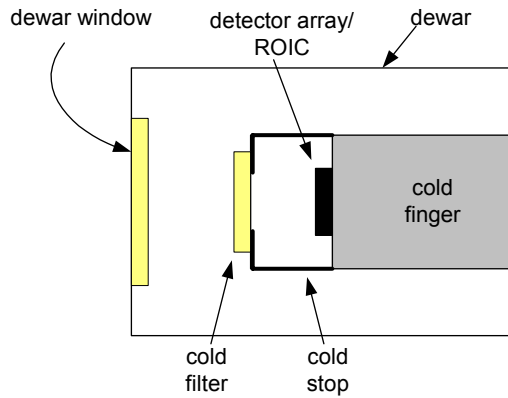


Figure 2: Typical FPA optical layout.

The cold stop and cold filter are used to reduce the straylight in order to keep the detector shot noise to a minimum value. Their temperature is generally the same as the detector array temperature. In addition to the étendue, the optical transmittance and the temperature of various components, the detector array parameters are important for the model. The detector responsivity, integration time, readout time, readout noise and dark current are these main parameters.

The last block from the system block diagram is the detector electronics and acquisition, where parameters like the amplifier noise and ADC (Analog-to-Digital converter) number of bits are from this block.

2. INPUT SCENE CHARACTERIZATION

In order to determine if an instrument is able to detect passively the presence of a gas, the first step is to calculate the radiance which is present at the input of the instrument¹. A typical scene layout is presented in Figure 3.

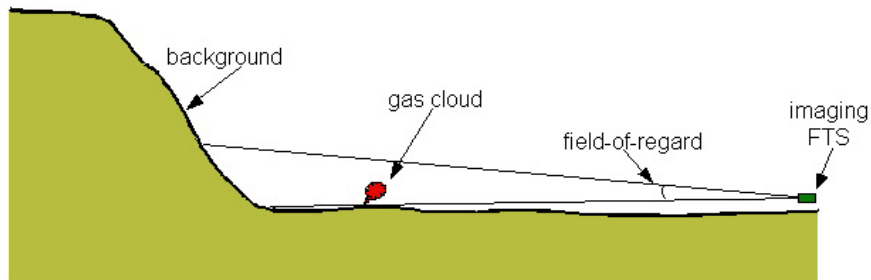


Figure 3: Typical scene layout.

Essentially, the instrument receives the radiance from the background that passes through a layer of air, a layer of the gas and another layer of air. To evaluate the contrast resulting from the presence of an absorbing gas when doing spectral radiance measurements, a simplified 3-layer model as described in Figure 4 is used.

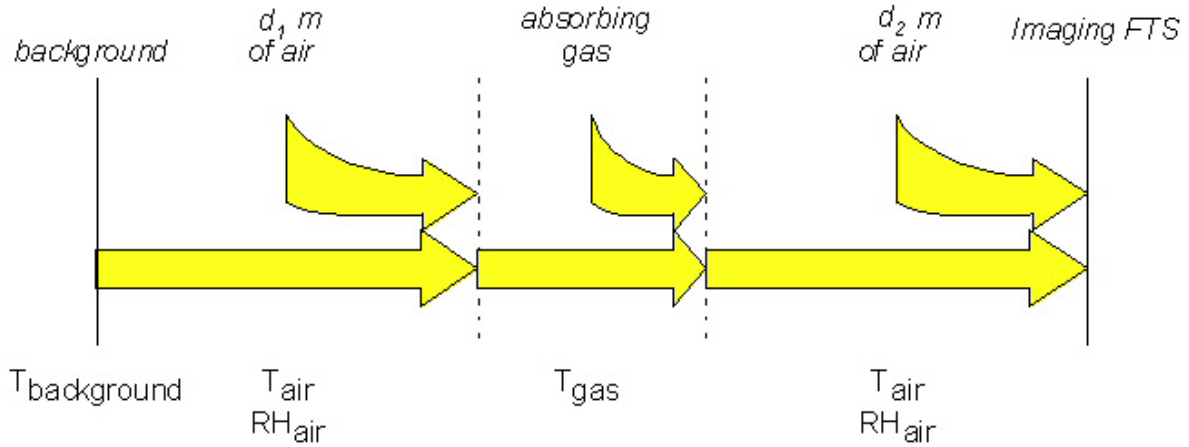


Figure 4: Radiative transfer model used to evaluate the impact of an absorbing gas on the spectral radiance.

The radiative transfer model implies that for each layer:

$$L_{out}(\sigma) = T_{layer}(\sigma)L_{in}(\sigma) + [1 - T_{layer}(\sigma)]L_{layer}(\sigma), \quad (1)$$

where $L_{out}(\sigma)$ is the spectral radiance at the output of the layer, $L_{in}(\sigma)$ is the spectral radiance at the input of the layer, $T_{layer}(\sigma)$ is the spectral transmittance of the layer and $L_{layer}(\sigma)$ is the spectral radiance of the gas inside the layer.

For the calculations in this paper, we simply assume that the background emissivity is 1. Its spectral radiance is thus that of a perfect black body. Each of the following 3 layers then absorbs some of the energy, while it emits according to its own temperature. Each layer is thus characterized by its temperature and its optical transmittance. The assumption of a perfect blackbody for the background is known to be unrealistic. However, when the background is known, one must use the known radiance of the background for the first layer, including reflected contributions.

2.1.1. Gas hotter than ambient air

We first evaluate the contrast of an absorbing gas when its temperature is higher than the ambient air. It corresponds to the case where the gas is just released from the stack (valid for a distance of few stack diameters).

Various temperature differences between air and background are considered, corresponding to typical scene conditions. They are the background temperature higher, equal and lower than the ambient air temperature. For these calculations, we assume 0.5 km of air between the background and the gas cloud, and 2.5 km between the gas and the instrument. The ambient temperature is 40°C. Figure 5 shows the observed contrast as a function of the gas temperature and the gas transmittance.

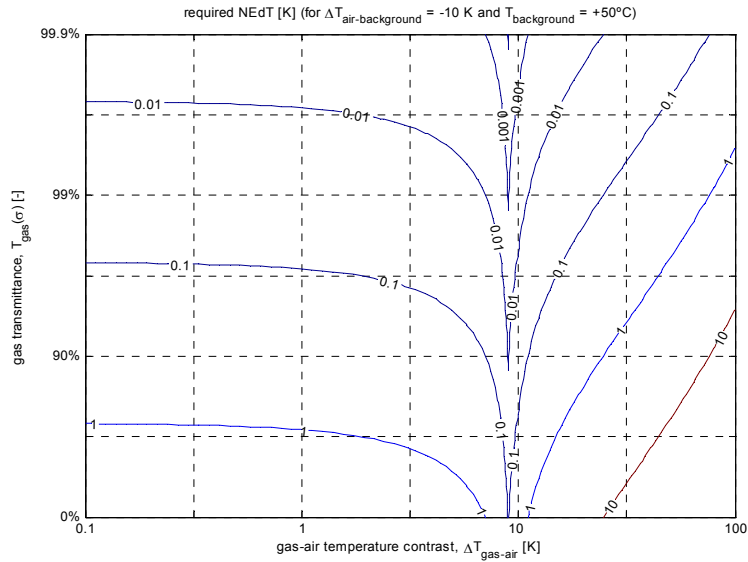


Figure 5: Contour plot giving the contrast brightness temperature (in K) corresponding to the contrast associated to the presence of the gas. The air is assumed 10°C colder than the background. The abscissa is the temperature difference between the gas and the air (on a log scale). The ordinate is the gas transmittance (on a log scale).

As an example, for a temperature difference of 1°C between gas and air, an instrument having a NEΔT of 0.1 K would enable the detection of the gas if it has a transmittance lower than 97.2% (conversely if it absorbs more than 2.8%), otherwise its absorption is too low and the instrument won't be able to detect it. When the gas is about 10°C hotter than the air, it reaches the temperature of the background, which makes its detection very difficult. It is not strictly 10°C since it is assumed for Figure 5 to Figure 7 that the air transmittance is 51%. On the other hand when the gas temperature is 100°C hotter than the air, its detection is easily achieved, since an instrument having a NEΔT of 0.1 K would enable the detection of the gas if it has a transmittance lower than >99.9%. Figure 6 and Figure 7 show the contrast brightness temperatures for different background temperatures, the ambient temperature being always 40°C.

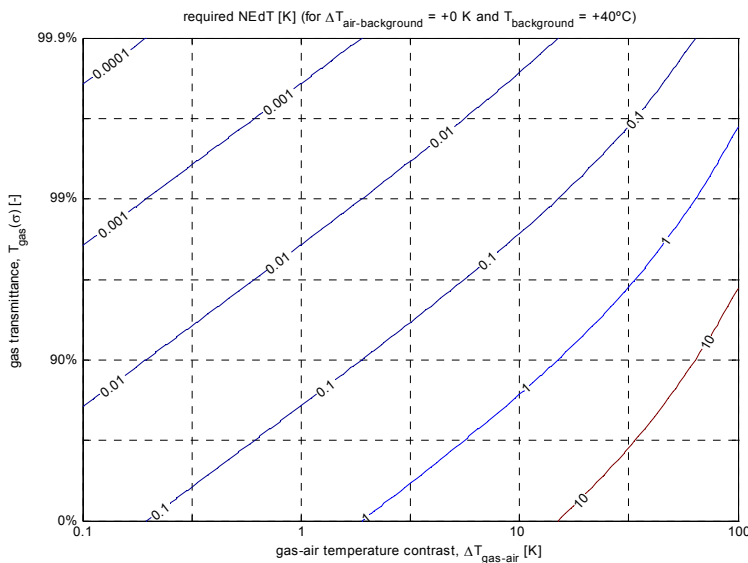


Figure 6: Contour plot giving the contrast brightness temperature (in K) corresponding to the contrast associated to the presence of the gas. The air is assumed at the same temperature than the background.

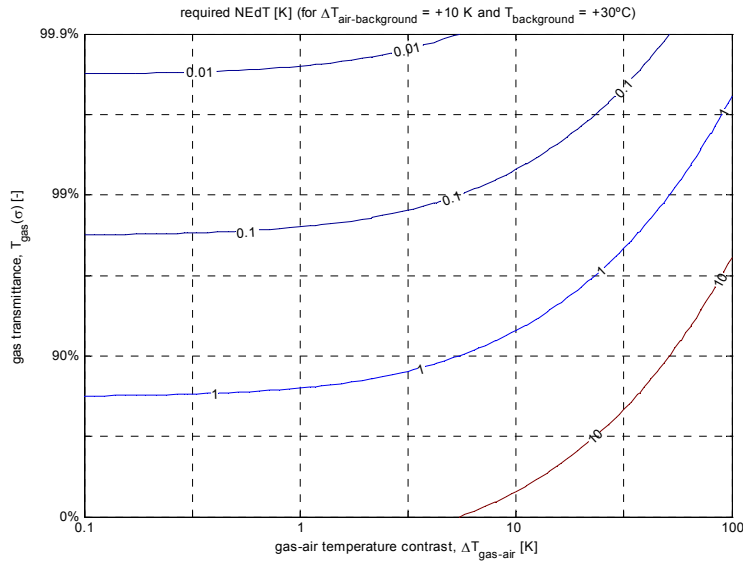


Figure 7: Contour plot giving the contrast brightness temperature (in K) corresponding to the contrast associated to the presence of the gas. The air is assumed 10°C hotter than the background.

2.1.2. Gas in thermal equilibrium with ambient air

We next evaluate the contrast of an absorbing gas when its temperature is similar to that of the ambient air. It corresponds to the case where the gas is away from the stack. Figure 8 depicts the required contrast to detect the gas as a function of the gas/air to background temperature difference and the gas transmittance. There is obviously no detection possible when all background/air/gas are at the same temperature (middle of the graph).

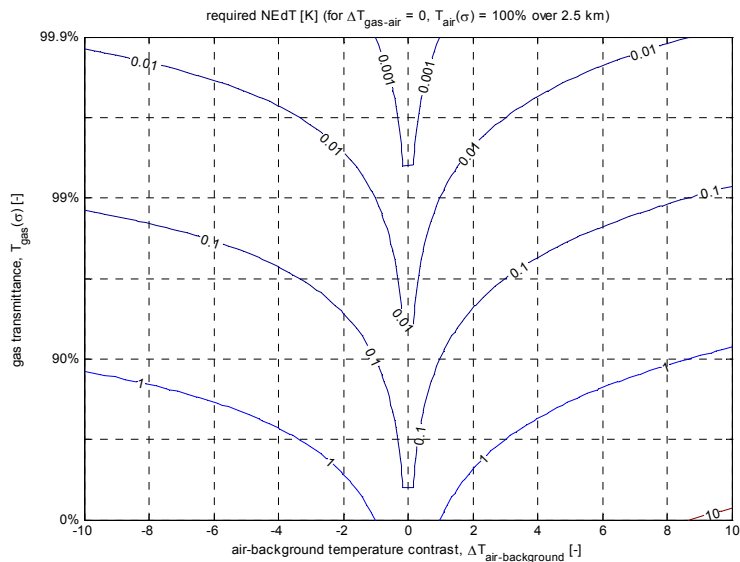


Figure 8: Contour plot giving the contrast brightness temperature (in K) corresponding to the contrast associated to the presence of the gas. The gas is assumed at the same temperature than the air. The air is assumed optically transparent. The abscissa is the temperature difference between the air/gas and the background (on a linear scale). The ordinate is the gas transmittance (on a log scale).

Figure 9 and Figure 10 show the contrast brightness temperatures when the air is more and more absorbing. The curves all have the same shape, while we notice that the required NE Δ T to detect the same amount of gas (same transmittance) slightly decreases, as the air is more opaque. For a transmittance of 38% over 2.5 km, the penalty is about a factor of 3.

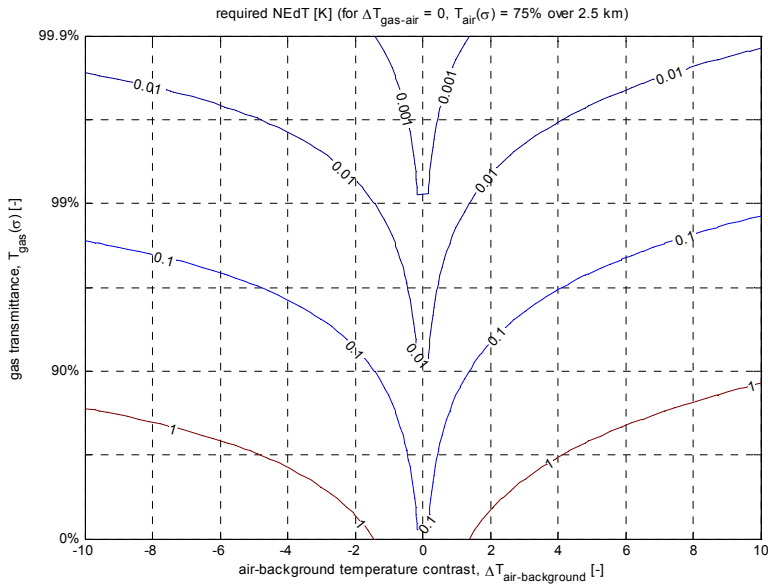


Figure 9: Contour plot giving the contrast brightness temperature (in K) corresponding to the contrast associated to the presence of the gas. The gas is assumed at the same temperature than the air. The air is assumed to transmit 75% over 2.5 km.

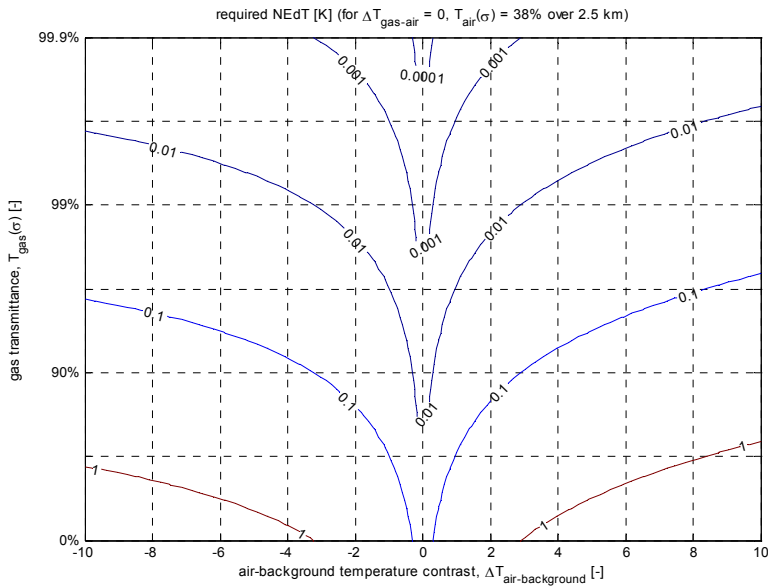


Figure 10: Contour plot giving the contrast brightness temperature (in K) corresponding to the contrast associated to the presence of the gas. The gas is assumed at the same temperature than the air. The air is assumed to transmit 38% over 2.5 km.

Table 1 summarizes the transmittance for the minimum amount of gas detectable for an instrument having an NE Δ T of 0.1 K. It shows that the detection threshold is about 3 times higher when air is transmitting 38% instead of 100%.

Table 1: Transmittance of minimum amount of gas detectable for an instrument having an NEdT of 0.1 K. Gas is at ambient temperature. Background is at 50°C. Air/gas temperature is 10°C away from background temperature.

air transmittance	maximum transmittance of gas detectable	minimum absorbance of gas detectable
100%	99.0%	1.0%
75%	98.6%	1.4%
51%	97.8%	2.2%
38%	96.9%	3.1%

3. TOTAL PHOTONS ON THE DETECTOR

Once the spectral radiance present at the input of the instrument determined, one has to calculate the total quantity of photons reaching the detector. The photons come from the scene and from the instrument itself. Careful attention should be paid to take into account the contribution of the second port of the interferometer. Figure 11 presents the approach.

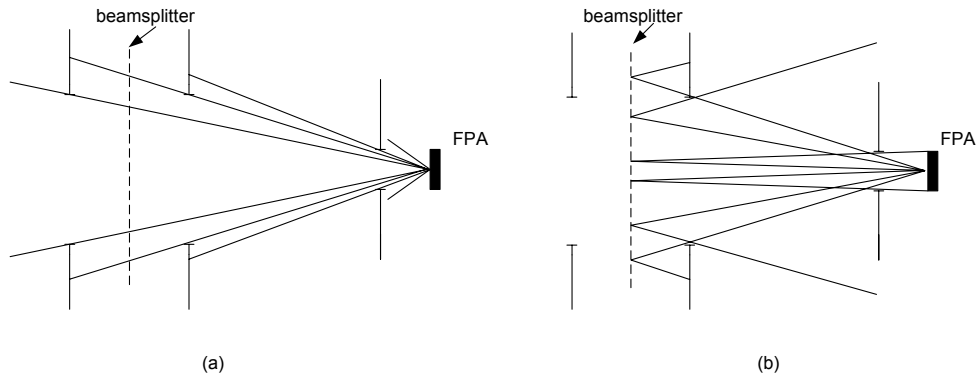


Figure 11: Determination of the total number of photons for a 2-port configuration; (a) main port contribution, (b) second port contribution.

For the 2-port configuration, the second port is the output port. The detector sees partially itself (narcissism effect). This reduces the photon flux level on the detector, which generally lowers the shot noise level. For a 4-port configuration, similar calculation is required. A different calculation has to be performed for each pixel of the detector. Some pixels might have vignetting and this should be taken into account. Figure 12 shows a typical configuration where an off-axis pixel has vignetting.

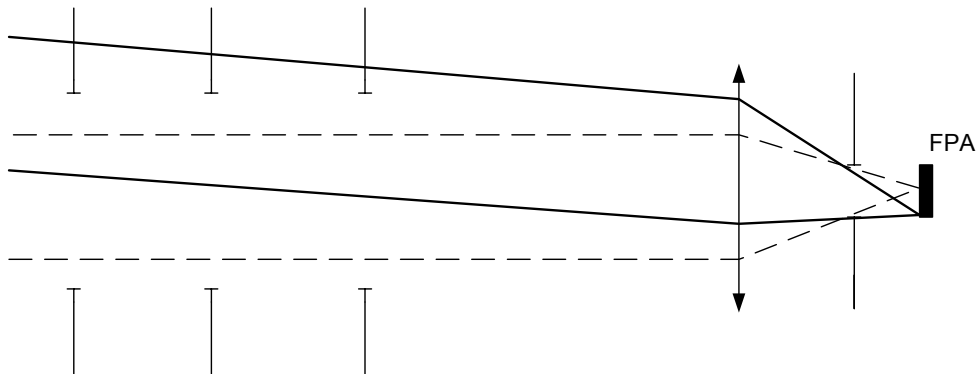


Figure 12: Center pixel has no vignetting (-- dashed line) and off-axis pixel with vignetting (- solid line).

The knowledge of the photon flux at the detector allows determining the optimal integration time taking into account the well capacity of the ROIC (Readout Integrated Circuit). The total photocurrent is also known, giving directly the detector shot noise. Étendue for the scene photons is now determined.

4. FPA OPERATING PARAMETERS

For imaging applications, where the number of pixels exceeds 64×64, the available detector arrays are mated to an ROIC. The ROIC has an accumulating well for each detector element. A standard sequence of operation for an ROIC is to empty the wells, integrate the photocurrent for a fixed duration and read sequentially each well. For optimal performance of the FTS, the integration of the photocurrent for each pixel must occur simultaneously (snapshot mode) and preferably synchronized to an OPD of the interferometer. ROICs have a few output taps with a maximum bandwidth. The readout rate (frame rate) is thus a limiting factor that must be taken into account when selecting the sweep speed of the interferometer. To meet the Nyquist criteria, the sampling distance in OPD must be smaller than one half of the smallest wavelength of the spectral band of the instrument. From the integration time plus the readout time of the ROIC, the average sweep speed of the interferometer is determined by:

$$\text{speed} = \frac{\text{sampling distance}}{\text{integration time} + \text{readout time}}. \quad (2)$$

The selection of the integration time has to take into account the well capacity as explained earlier in section 3, and also the low pass filtering effect of this integrator:

$$h(\sigma) = t_{\text{int}} \text{sinc}(t_{\text{int}} \cdot \text{speed} \cdot \sigma). \quad (3)$$

Finally, it is always interesting to verify the data rate of the analyzed system. For a frame rate of 1 kHz, a 128×128 imaging FTS generates 250 Mbits/sec of data that must be acquired and processed.

5. SAMPLING JITTER

The imaging FTS using an integrating FPA as presented in section 4 gives perfect results when the speed is constant. For a step-scan, speed fluctuations are not present and time jitter is directly replaced by OPD jitter. However, since the FPA operates on a time varying signal and the interferogram is a position dependant signal, the presence of speed fluctuations gives rise to additional noise in the measured spectra because of sampling jitter². Figure 13 presents the nominal and realistic conditions of an FPA operation.

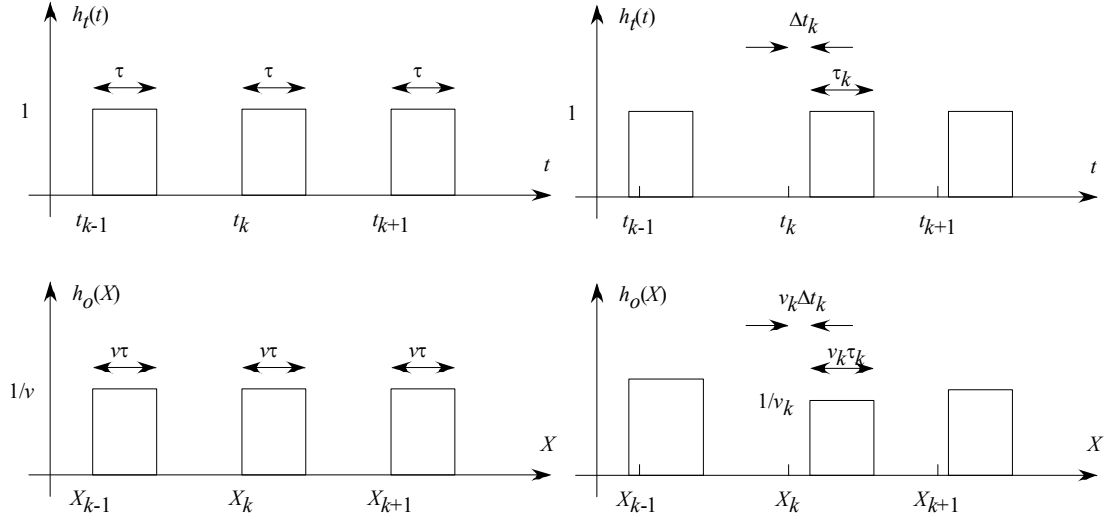


Figure 13: Illustration of the time-domain and the OPD-domain impulse responses of an integrating camera under nominal conditions (left) and under realistic conditions (right) where random jitter, integration time and velocity are depicted.

Detailed stochastic analysis allows calculating the level of noise as a function of the speed, delay and integration time fluctuations. For small fluctuations and under the assumption of mutual independence, the total noise is obtained from the sum of the individual noise contributions:

$$\left(\frac{NESR}{S(\sigma)}\right)^2 = \frac{\text{var}\{\hat{S}(\sigma)\}_{\Delta t}}{|E\{\hat{S}(\sigma)\}_{\Delta t}|^2} + \frac{\text{var}\{\hat{S}(\sigma)\}_v}{|E\{\hat{S}(\sigma)\}_v|^2} + \frac{\text{var}\{\hat{S}(\sigma)\}_\tau}{|E\{\hat{S}(\sigma)\}_\tau|^2}. \quad (4)$$

Figure 14 presents the results for an interferometer speed of 0.25 cm/s and nominal integration time of 100 μ s.

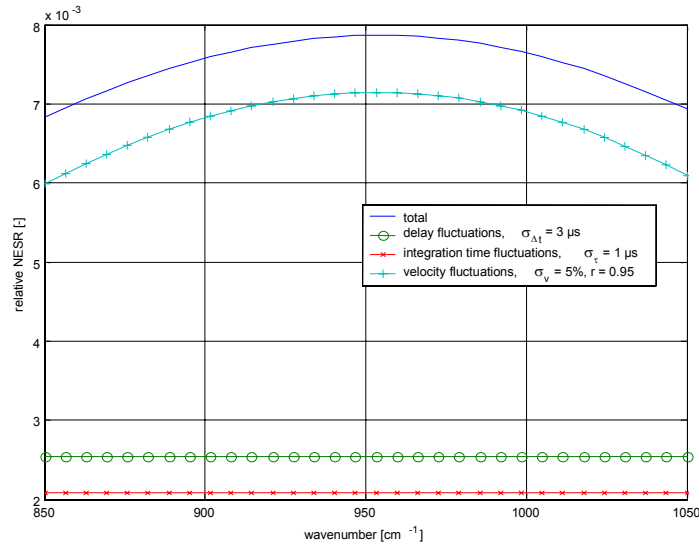


Figure 14: Calculation of relative standard deviation of the spectrum estimator for an FTS with an integrating camera operating simultaneous under delay, integration time and velocity fluctuations.

In this example, the noise is dominated by the speed fluctuations and the highest noise is in the middle of the band at 0.8% of the scene radiance. A uniform narrow spectral radiance is assumed ranging from 850 to 1050 cm^{-1} .

6. UNCOMPENSATED CONFIGURATION

For an imaging FTS, people consider the use of an uncompensated interferometer to spread the ZPD region of the interferogram (dispersion), thus reducing the dynamic range of the signal. That way, longer integration time can be used before saturating the well and the number of bits of the ADC can be reduced. However, an important phenomenon occurs for uncompensated interferometers. This has been presented in details by R. Desbiens *et al.*³ and the key conclusions are reproduced here in Figure 15.

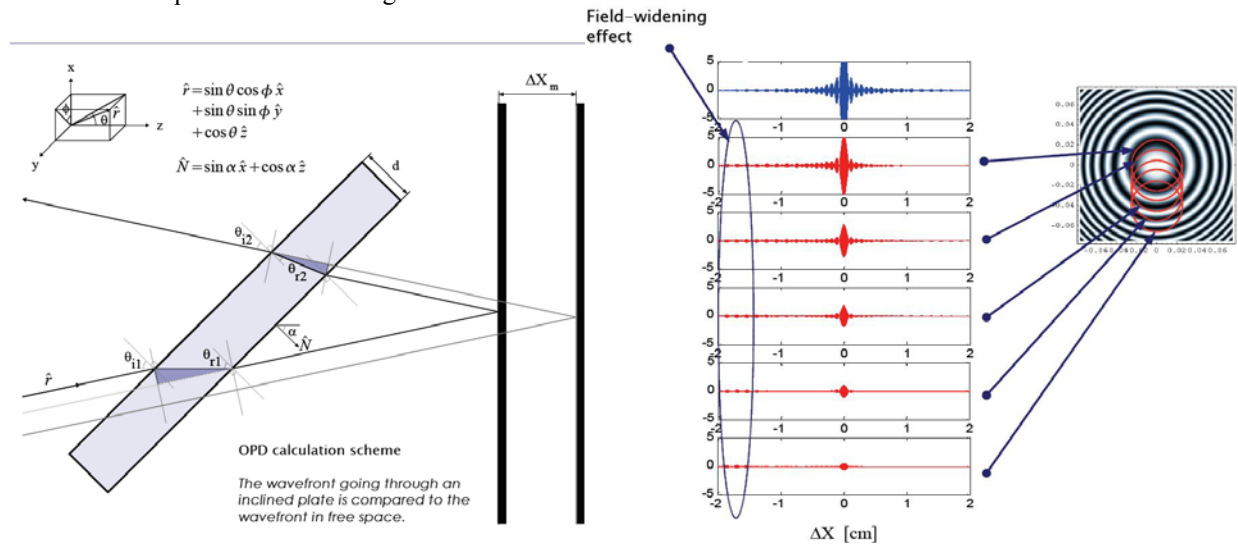


Figure 15: The optical path length going through the plate is compared to the one in free space (left); circular fringes are present in the image plane at ZPD for an uncompensated configuration (right) resulting in a loss of modulation³.

An uncompensated interferometer has a ZPD (Zero optical Path Difference) that depends on the angle of the rays going through the beamsplitter plate. This produces fringes in the image plane, even at ZPD and its vicinity. Each detector element integrates portion of this intensity pattern. The presence of the fringes may strongly reduce the modulation efficiency. The larger the detector element the higher is the loss in modulation. Moreover, for a given detector size, modulation efficiency decreases when going off-axis. To predict the performance of the imaging FTS, modulation efficiency has to be calculated taking this phenomenon into account.

7. NESR MODEL

Telops has developed a complete model to predict the NESR performance of imaging FTS. The model requires an important number of inputs as described in this paper. Figure 16 presents a table with the various required inputs. Figure 17 shows the output of the model where the various contributors are breakdowned to determine which one is the dominant. In this example, the noise is dominated by the shot noise from the photons.

Inputs for NESR Estimations - SPIE paper					Inputs for NESR Estimations - SPIE paper				
	Description	Value	Units	Comment		Description	Value	Units	Comment
Scene	Scene Temperature	300	K	Nominal	Detector	Oversampling	0	-	
	Reference Temperature	300	K	Same as Temperature for derivation		Transmission	1	-	Nominal
	Instantaneous FOV	1	mrad			Integration time	0.000100	s	
Fore Optics	Measurement Duration	8.1	s	Calculated		Noise Contributions	0	sqrt(Hz)	Nominal
	Telescope Temperature	300	K	Nominal		Quantum efficiency	0.6	-	Nominal (MCT)
	Diameter of Entrance Aperture	4	cm			Temperature of Optics	300	K	Nominal
	Magnification	1	-			Dark Current	5.00E-06	mA	Nominal
	Transmission	≈ 0.95	-	Input Window -> ZnSe Ar-coated		Readout noise	1000	electron	RMS, Nominal
Interferometer	Shape of entrance aperture	circle'	-	Can be either 'circle' or 'square'		Number of bits / ADC	14	-	Nominal
	Maximum Path Difference	0.25	cm	double-sided sweep		ADC Security Range	20	%	Nominal
	Transmission	≈ 0.83	-	Varies across range [8 - 12] μm		FPA Height	128	-	Nominal
	RMS Wavefront Distortion	1.33E-05	cm	Nominal, lambda/5 @ HeNe		FPA Width	128	-	Nominal
	Beamsplitter reflectance	≈ 0.50	-	Wavenumber dependant		Shape of detector	'square'	-	Nominal
	Beamsplitter transmittance	≈ 0.50	-	Wavenumber dependant		FPA Off axis X error	0	mrad	
	Sampling time interval	1.00E-03	s	FPA frame rate		FPA Off axis Y error	0	mrad	
	Sweep reversal duration	2.50E-02	s	Nominal		Pitch between pixels	25	um	Nominal
	Co-Addition of IGMs	4	-	Nominal		Electron Well Capacity	2.50E+07	electron	Nominal
	Sampling Interval	2.5	μm	Nominal		Temperature of detector	77	K	Nominal
Aft optics	OPD Dependant Average WF Tilt	1.00E-05	cm rad	Nominal		Integration time period fluctuation	1.00E-06	s	
	RMS Wavefront Tilt	0	rad	Nominal		Integration time delay fluctuation	3.00E-06	s	
	OPD Dependant average WF Shear	[-25e-6 25e-6]	cm cm	Nominal		Numerical apodization	'BoxCar'	-	Nominal
	Temperature of Interferometer	300	K	Nominal		Channel Centers Definition	-	um	
	Average Sweep Speed	0.25	cm/s	= 2MPD / Startetime		Channel Bandwidth	-	um	
	Speed Deviation	5	%			Channel Tolerance	-	um	
	Coefficient of correlation	0.95	-	sample to sample		Channel Maximum NEdT	-	K	
	Temperature of Aft-Optics	300	K	Nominal		Decimation Factor	xx	-	
	Cold Filter Tx	0.9	-			Spatial Binning	1	-	Nominal
	Lens Tx	≈ 0.97	%	ZnSe Lens		Temperature	77	K	Nominal
Band	Window Tx	≈ 0.94	%	ZnSe Window		Location of Aperture Stop	D'	-	Nominal
						Surface Over Aperture Stop	0	%	Nominal
					Lower bound	833	cm-1	Nominal	
					Higher bound	1250	cm-1	Nominal	

Figure 16: Table of inputs for the NESR model.

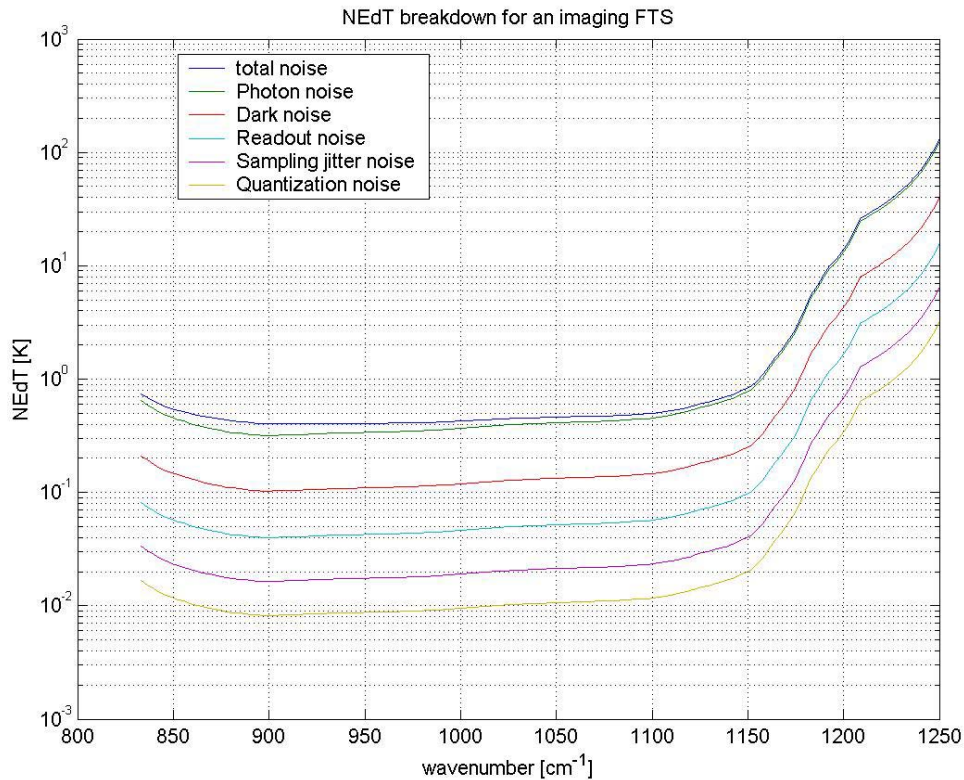


Figure 17: NEdT and the breakdown of the different contributors.

The noise level can be compared to the required contrast as calculated earlier in section 2.

8. CONCLUSIONS

In this paper, we presented the modeling of the scene to determine the input radiance and the contrast from the gas to measure. Careful determination of the photon flux reaching the detector is important. A complete model is used to predict the noise from various contributors. The presented ensemble of design tools enables to easily define instrument requirements and predict performance for imaging FTS application in chemical standoff detection.

ACKNOWLEDGMENTS

The authors would like to thank Michael Dobbs and Merritt Webb from ITT Industries (ITT Aerospace/Communications, Fort Wayne, IN) for their collaboration in the use and validation of the models developed for imaging FTS applications, and for funding part of this study.

REFERENCES

1. J.-M. Thériault, *Passive standoff detection of chemical vapours by differential FTIR radiometry*. DREV Technical Report TR-2000-156, UNCLASSIFIED, 2001.
2. L. Palchetti, D. Lastrucci, *Spectral noise due to sampling errors in Fourier-transform spectroscopy*, Appl. Opt. 40(19), 3235-3243, 1 July 2001.
3. R. Desbiens *et al.*, *Field Widening Effects on Modulation Efficiency and ILS Resulting From the Use of Uncompensated Beam Splitter*, ASSFTS-11, Germany, October 2003.